Energy Conversion and Management 248 (2021) 114808

Contents lists available at ScienceDirect

Energy Conversion and Management

journal homepage: www.elsevier.com/locate/enconman

Optimal energy management system using biogeography based optimization for grid-connected MVDC microgrid with photovoltaic, hydrogen system, electric vehicles and Z-source converters

Lais de Oliveira-Assis [a], Pablo García-Triviño [a], Emanuel P.P. Soares-Ramos [a,b], Raúl Sarrias-Mena [c], Carlos Andrés García-Vázquez [a], Carlos Ernesto Ugalde-Loo [d], Luis M. Fernández-Ramírez [a,*]

[a] Research Group in Sustainable and Renewable Electrical Technologies (PAIDI-TEP023), Department of Electrical Engineering, Higher Technical School of Engineering of Algeciras (ETSIA), University of Cádiz, Avda. Ramón Puyol, s/n., 11202 Algeciras, Cádiz, Spain
[b] Federal Center for Technological Education of Minas Gerais, Department of Electro-electronics, R. Raymundo Matoso, 900, Santa Rita, Curvelo, MG 35790-000, Brazil
[c] Research Group in Sustainable and Renewable Electrical Technologies (PAIDI-TEP023), Department of Engineering in Automation, Electronics and Computer Architecture & Networks, Higher Technical School of Engineering of Algeciras (ETSIA), University of Cádiz, Avda. Ramón Puyol, s/n., 11202 Algeciras, Cádiz, Spain
[d] School of Engineering, Cardiff University, CF24 3AA Cardiff, U.K

ARTICLE INFO

Keywords:
Microgrid
Hydrogen system
Electric vehicles
Power converters
Energy management system

ABSTRACT

Currently, the technology associated with charging stations for electric vehicles (EV) needs to be studied and improved to further encourage its implementation. This paper presents a new energy management system (EMS) based on a Biogeography-Based Optimization (BBO) algorithm for a hybrid EV charging station with a configuration that integrates Z-source converters (ZSC) into medium voltage direct current (MVDC) grids. The EMS uses the evolutionary BBO algorithm to optimize a fitness function defining the equivalent hydrogen consumption/generation. The charging station consists of a photovoltaic (PV) system, a local grid connection, two fast charging units and two energy storage systems (ESS), a battery energy storage (BES) and a complete hydrogen system with fuel cell (FC), electrolyzer (LZ) and hydrogen tank. Through the use of the BBO algorithm, the EMS manages the energy flow among the components to keep the power balance in the system, reducing the equivalent hydrogen consumption and optimizing the equivalent hydrogen generation. The EMS and the configuration of the charging station based on ZSCs are the main contributions of the paper. The behaviour of the EMS is demonstrated with three EV connected to the charging station under different conditions of sun irradiance. In addition, the proposed EMS is compared with a simpler EMS for the optimal management of ESS in hybrid configurations. The simulation results show that the proposed EMS achieves a notable improvement in the equivalent hydrogen consumption/generation with respect to the simpler EMS. Thanks to the proposed configuration, the output voltage of the components can be upgraded to MVDC, while reducing the number of power converters compared with other configurations without ZSC.

1. Introduction

A microgrid is "a group of Distributed Energy Resources (DER), including Renewable Energy Sources (RES) and ESS, plus loads that operate locally as a single controllable entity" [1].

RES, mainly solar and wind energy, are non-dispatchable DER because the energy resource is uncontrollable. The electrical generation from RES is intermittent (generation is not possible at any time, only when the energy resource is available), fluctuating and uneven over time due to the inherent characteristics of energy resource. ESSs are an interesting option to help mitigating these drawbacks, increasing generation capacity and gaining energy support/storage capability [2]. Microgrids with RES and ESS can operate efficiently and effectively when the available energy and/or demand change, since RES generation can be stored into the ESS and the stored energy can be recovered when needed [3].

Batteries are one of the most used ESS in microgrids because they are cost-effective, modular and easy to implement [4]. Hydrogen systems based on LZ and FC are another interesting ESS for microgrids. The LZ

* Corresponding author.
E-mail address: luis.fernandez@uca.es (L.M. Fernández-Ramírez).

https://doi.org/10.1016/j.enconman.2021.114808
Received 16 July 2021; Accepted 26 September 2021
Available online 2 October 2021

Nomenclature

3.1 ZSC

B *and* G Voltage gain factor in the qZSI and in the ZSC
D *and* D_c shoot-through period in the qZSI and in the ZSC
I_{BES} BES current
$I_{in.ZSC}$ *and* $I_{out.ZSC}$ Input and output current in the ZSC
I_{in} *and* I_{dc} Input and output current in the impedance network
$i_a(t), i_b(t), i_c(t)$ Three-phase current
$m_a(t), m_b(t), m_c(t)$ Three-phase modulating signals
P_{BES} BES power
P_{H2} Hydrogen system power (FC or electrolyzer
P_{PV} PV system power
P_{dc} Out power after the impedance network
P_{grid} GRID power
V_{BES} BES voltage
V_{C1} *and* V_{MVDC} Voltage in C1 (MVDC)
$V_{in.ZSC}$ *and* $V_{out.ZSC}$ Input and output voltage in the ZSC
V_{in} *and* V_{dc} Input and output voltage in the impedance network
$v_a(t), v_b(t), v_c(t)$ Three-phase voltage

3.2 Hydrogen System

CAP Nominal capacity of the hydrogen tank
E_{cell} *and* E^0_{cell} Nernst's instantaneous voltage and standard-state reversible voltage
F Faraday's constant
I_{LZ} Electrolyzer current
k_e Constant (function of the entropy change)
L_{H2} *and* $L_{H2,0}$ Hydrogen tank level and initial level
p_{H20}, p_{H2}, p_{o2} Partial pressures of the water, hydrogen and oxygen
Q_{H2} Hydrogen generated or consumed by the FC or LZ
R Ideal gas constant
R_i Slope of the linear variation under given conditions (LZ model)
R_{i0} Internal resistance of the LZ
T and T_0 Working operation and reference operation temperature of the FC and LZ.
V_{FC} *and* V_{LZ} FC and electrolyzer voltage
V_{act} *and* V_{ohm} Activation and ohmic drop voltage in the FC
V_{irrev} Irreversible voltage
V_{rev} Minimum voltage in the LZ needed to produce a current flow
V_{rev0} Reference value for the reverse voltage

3.3 Batteries models (BES and EV)

I_{bat} Battery current
Q Maximum battery capacity
R_{int} Internal resistance of the batteries
SOC *and* SOC_o State of charge and initial state of charge of the batteries
V_{bat} *and* E_{bat} Output voltage and open circuit voltage of the batteries

3.4 PV System

G_s *and* G_n Irradiation on the device surface and the nominal irradiation
I_L *and* I_{L0} Solar-induced current and solar-induced current at 300 K
I_{PV} PV system current
I_{sat} Saturation Current of a diode
K_1 and K_0 Constants depending on the PV characteristic
k Boltzmann constant
N Quality factor of the diode of the PV model
q Elementary charge of an electron
T_{PV} Operating temperature of the PV
R_s *and* R_{sh} Series and shunt resistance
V_g Voltage applied to the terminals of the diode

4.1 Fitness function: Equivalent hydrogen consumption and generation

K Penalty coefficient of hydrogen consumption
LCV_{H2} and HCV_{H2} Low calorific value and 'high calorific value
L^{min}_{H2} *and* L^{max}_{H2} Minimum and maximum hydrogen level in the tank
$P_1 \cdots P_5$ Coefficients of the FC and LZ efficiency polynomic
P^{min}_{BES} *and* P^{max}_{BES} Minimum and maximum power of the BES
P_{EV} Power consumed by the EV
P_{FC} *and* P_{LZ} FC and LZ power
P^{avg}_{FC} and P^{avg}_{LZ} average FC and LZ power
P^{nom}_{FC} *and* P^{max}_{FC} Nominal and maximum power of the FC
P^{nom}_{LZ} *and* P^{max}_{LZ} Nominal and maximum power of the LZ
P_{NET} Net power
$Q_{BES,con}$ and $Q_{BES,gen}$ Equivalent hydrogen consumption and generation of the BES
$Q_{H2,FC}$ and $Q_{H2,LZ}$ FC hydrogen consumption and LZ hydrogen generation
$Q^{avg}_{H2,FC}$ and $Q^{avg}_{H2,LZ}$ Average hydrogen consumption of the FC and average hydrogen generation of the LZ
$Q^{eq}_{H2,con}$ *and* $Q^{eq}_{H2,gen}$ Equivalent hydrogen consumption and generation
$q^{nom}_{H2,LZ}$ Nominal hydrogen flow generation of the LZ
R_{BES} Internal resistance of the BES
SOC_{min} *and* SOC_{max} Minimum and maximum SOC of the BES
U^{min}_{BAT} *and* U^{max}_{BAT} Minimum and maximum voltage of the BES
U_{BES} Open circuit voltage of the BES
U_f Utilization factor
η_{FC} and η_{LZ} FC and LZ efficiency
η_{char} *and* η_{dis} Charge and discharge BES efficiency
η^{avg}_{char} *and* η^{avg}_{dis} Average charge and discharge BES efficiency
η_{ther} Thermodynamic efficiency of the FC
μ_{SOC} Charging and discharging coefficient performance of the BES
E *and* I maximum emigration rate and maximum immigration rate
m_{max} maximum mutation rate
P_{max} maximum mutation probability
P_s mutation probability
S_0 *and* S_{max} Number of species that gets the equilibrium and maximum number of species
λ *and* μ immigration and emigration rates

4.3 Control loops

FCU Fast charging unit
I_{FC} *and* I_{LZ} FC and LZ current
I^{ref}_d *and* I^{ref}_q Reference grid current (dq frame)
M Module of index modulation
m_d *and* m_q dq components of the index modulation
V^{nom}_{BES} Nominal voltage of the BES
V^{MPPT}_{PV} MPPT voltage of the PV system
ΔD *and* Do Control terms for D

consumes renewable electricity to produce hydrogen from water (green hydrogen), which is stored into a hydrogen tank [5]. The hydrogen stored can be transformed into electricity by a FC and also used as an energy source for domestic, commercial, industrial or mobility purposes. ESSs based on hydrogen have advantages such as long storage times and high capacities, as well as the potential for producing both electricity and heat with low environmental impact [6]. The main drawback is their high capital cost compared with other ESSs like batteries, although there are multiple initiatives worldwide to promote their development [78] that are helping to reduce their cost [9].

The efforts to decarbonize transport are promoting the development and use of EV, making them and their charging stations one of the most common loads in microgrids. Hence, the integration of EV charging stations into microgrids with RES and ESS allows optimizing RES generation, storing it into ESS to charge EV, while trying to make the microgrid as self-sufficient as possible, providing peak shaving and more reliability to the grid [10].

DC microgrids are becoming a growing solution for integration of RES, ESS and EV into residential, commercial and industrial applications [11]. Compared with the traditional AC grids, DC grids present higher reliability and efficiency, cost reduction and simplicity, avoiding some issues such as reactive power flow, synchronization, frequency regulation and harmonics [12]. Hence, a microgrid for a PV based EV charging station was used for a workplace parking garage in [13], where the economic and emission impacts were studied, comparing an optimal charge scheduling strategy with an uncontrolled charging case, evidencing the feasibility of this configuration and the importance of an optimal charge controller. Another example of microgrid combining RES, ESS and EV was presented in [14], in which a fast-charging station was proposed with its respective optimization, in order to maximize the profit measured by the net present value.

These works are based on the use of LVDC microgrids. However, when power and voltage levels increase, MVDC microgrids represent an interesting solution because they allow reducing the number of conversion stages, and thus, minimizing power conversion and improving efficiency. Moreover, they facilitate the integration of large- and small-scale microgrids with RES, ESS and EV into the electrical grid operating at a higher voltage [15].

Traditional DC/DC converters and AC/DC converters based on voltage source inverters are commonly used in microgrids. A DC/DC boost converter connects each DC energy source and load (RES like PV and ESS, and EV) to a common DC bus, and a voltage source inverter transforms DC into AC voltage for the grid integration. This configuration is based on a two-stage conversion system (DC/DC boost converter plus DC/AC voltage source inverter). However, single-stage conversion is an attractive option due to its reduced losses, low device count and lower costs [16]. ZSC present a specific configuration based on an impedance network that allows a large voltage buck-boost feature in a single-stage conversion [17].

The microgrids integrating RES, ESS and EV charging stations require an EMS to properly control the energy flow between the energy sources and the grid. A complete review of EMS strategies for hybrid renewable systems was performed in [18], where different control approaches were discussed, such as linear programming and intelligent techniques for standalone and grid connected systems. Hence, optimizing the EMS can contribute to ensure a better use of the available resources and ensure the continuity of load supply.

In this context, BBO algorithm, which is a method based on the study of geographical distribution of species, was first proposed as optimization method in [19]. BBO can be used in several applications such as optimization of the fuzzy membership functions to generate a proper duty cycle for the maximum power point tracking (MPPT) control [20], the optimization of a neural network for long-term forecasting of the energy demand [21], and for charging pattern optimization for lithium-ion batteries [22], proving to be a powerful method for handling complex optimization issues.

In this paper, a microgrid composed of PV panels, hydrogen system (FC, LZ and tank), BES and two fast charging stations for EV is considered. The energy sources are connected to a common MVDC bus and the grid through the ZSC. A new EMS using an optimization algorithm based on BBO is proposed and compared with a traditional EMS based on states, achieving better results in the consumption and generation of hydrogen, and therefore, in the energy management of the microgrid. The main contributions of this paper lie in the configuration of the microgrid based on ZSC and in the EMS based on the BBO algorithm.

The present work is organized as follows. The microgrid under study is presented in Section 2. The modelling of this microgrid is illustrated in Section 3. In Section 4, the proposed EMS based on the BBO algorithm is described. The simulation results are presented in Section 5, and finally, the conclusions are drawn in Section 6.

2. MVDC microgrid with PV, hydrogen system, batteries, EV and ZSC

The aim of the MVDC microgrid is to supply the energy demanded by the batteries of the EV connected to it. Although the system is connected to the utility grid, in normal conditions it works as a standalone microgrid. The PV system is the main energy source and two ESS, the BES and the hydrogen system, are in charge of adjusting generation and consumption, keeping the power balance in the microgrid. Only in the case when the power balance cannot be kept by the microgrid energy sources, the grid ensures it, avoiding any functional problem.

Fig. 1 shows the whole configuration of the proposed microgrid. The main source of the system, the PV system, must have a peak power above the rated power (two fast charging unit of 50 kW each one). Thus, the solar panel Sunpower SPR-X21-335 (335 W) [23] is grouped in a 55x16 structure to reach a PV peak power of 186 kW, with an output voltage of 615 V. Besides, the charging station includes two ESSs: a BES and a complete hydrogen system (FC, LZ and hydrogen tank). Both ESSs help the PV system to supply the energy demanded by the charging station and stabilize the system when working in isolated mode (normal condition). The BES is the Hoppecke Sunpower OPZV lead-acid battery for cycling applications [24], with a rated capacity of 76.45 kWh and a bus voltage of 615 V. The hydrogen system, which can be considered a bidirectional storage system, is composed of 6 Hydrogenics HyPM HD power modules [25], with a 66 kW of peak power, a Proton OnSite C20 Hydrogen Generation System with a maximum power of 176 kVA [26] and a metal hydrogen tank of 450 kg.

On the other side, the power demanded to charge the batteries of the EV is considered the system load. In this work, the hybrid charging station has two fast charging units that incorporate an off-board charger unit with a ZSC to control the charge of each EV, which present the following features: EV charging mode 4, IEC61851-1 [27], rated power 48 kW, fast charging with external charger in DC, voltage up to 500 V, and current up to 200 A. In this case, Li-on cell batteries have been considered, with a rated capacity of 20 kWh.

ZSC are used to integrate the energy sources into a common MVDC bus and connect them to the grid. The main ZSC is a quasi-Z-source inverter (qZSI) made up of an impedance network and an inverter [28]. This converter is used to link the PV system, the BES and the local grid in AC. The PV system is connected at the DC side of the qZSI, the BES is in parallel with its impedance network, and the grid at the AC side of the qZSI. The MVDC bus (around 1550 V) is obtained from the impedance network of the qZSI, where the other energy sources are connected through ZSC. Thus, three ZSC designed and developed in [29] have been included in this configuration: one ZSC for the hydrogen system and two ZSC for the fast charging units. These converters are used due to their advantages to adapt voltage levels and reduce the number of power converters [17].

Thanks to this configuration, the output voltages of the components can be adapted to MVDC to control their output power and reduce the number of power converters compared with the common configuration

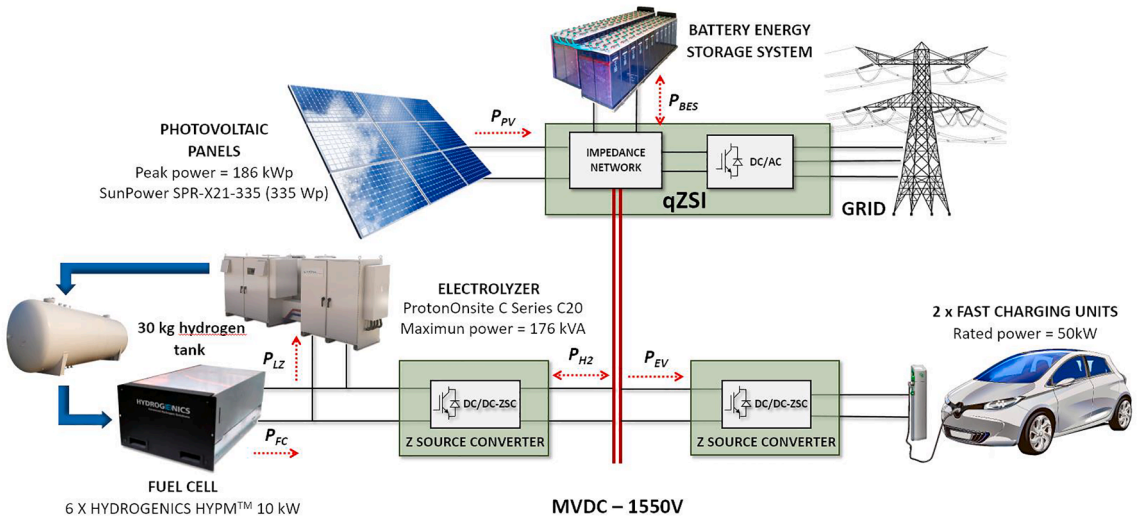

Fig. 1. Configuration of the grid-connected MVDC microgrid with PV, hydrogen system, EV and ZSC.

without ZSC. Thus, in a plausible configuration without ZSC, in addition to replacing the ZSC by conventional DC/DC converters, two additional DC/DC converters should be included, one to control the PV system and another one to control the BES.

3. Modelling of the grid-connected MVDC microgrid

This section illustrates the modelling of the components that integrate the microgrid. Nevertheless, since the novelties reside in the use of the ZSC to connect the energy sources to the microgrid and the equivalent hydrogen consumption to manage the microgrid, the modelling of the ZSC and hydrogen system are developed more in detail than the others (see sections 3.1 and 3.2, respectively).

3.1. ZSc

Detailed models (or fully-switched model) of the ZSC based on switches and impedances can be replaced by less complex models, called averaged models. In these models, the impedance network, the switches of the ZSC, or both, are represented by controlled current and voltage sources, which, over one cycle of the switching frequency, generate the current and voltage averaged values. They can represent the low-frequency response of the converters in dynamic studies and for control purposes, long-term simulations, and modeling and simulation of large power systems, but they do not represent the current and voltage harmonics.

Because of the simplicity of the averaged models, the sample time can be increased, resulting in a faster simulation and lower simulation rate (lower computational efforts), while maintaining an appropriate accuracy that does not affect the value of the input and output power of the ZSC. A comparison was carried out in [30] between averaged and full-switched models, with results confirming that averaged models are perfectly adequate for the needs of the present work. Hence, an averaged model of the qZSI (averaged qZSI) is used in this work to connect the PV panels to the grid, and an averaged model of a DC/DC ZSC (averaged ZSC) is used to link the hydrogen system and the batteries of the EV to the MVDC bus. [30]

3.1.1. Averaged model of the qZSI

The qZSI is modelled by controlled voltage and current sources that replace the impedance network and the switches of the inverter (Fig. 2). These controlled sources are interrelated through the boost factor (B) and the modulating signals ($m_a(t)$, $m_b(t)$ and $m_c(t)$). Thus, this model is based on the knowledge of B and $m_a(t)$, $m_b(t)$ and $m_c(t)$. Section 3.4 shows the control strategies implemented on them.

Note that in the qZSI models presented, the pulses of switches are not considered. Due to this simplification, the data processing requirements are reduced notably (the time step is increased), while the final results are quite similar to a fully-switched model. The models presented do not show the behavior of the current and voltage harmonics, but they do represent the dynamic performance of the qZSI, which is especially important when the power flow among the components of the microgrid

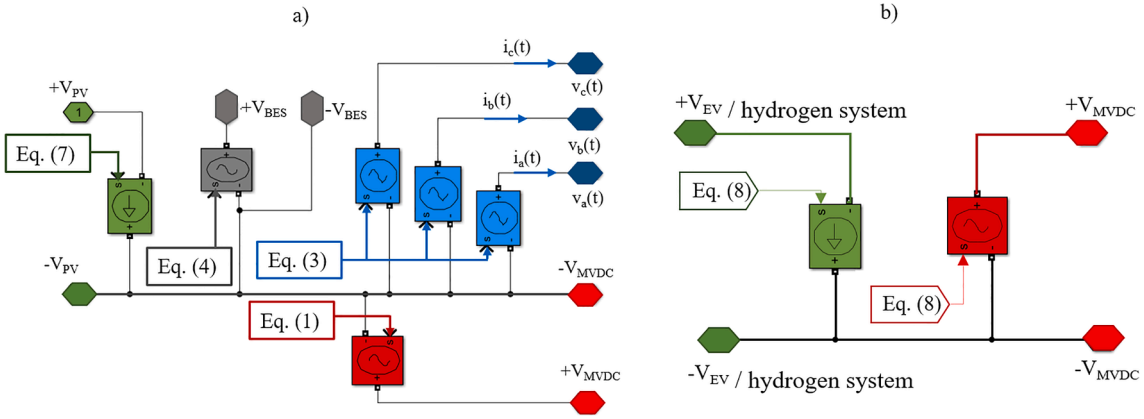

Fig. 2. a) Averaged model of the qZSI and b) averaged model of the DC/DC ZSC.

must be properly managed, as in this work.

In a lossless qZSI, the input voltage (V_{in}) and the voltage across the capacitor C_1 (V_{C1}) or MVDC bus voltage (V_{MVDC}) are related through Eq. (1), where D is the shoot-through period. Eq. (2) shows the relation between V_{in} and the output voltage of the impedance network (V_{dc}). V_{dc} and the AC voltages are related through $m_a(t)$, $m_b(t)$ and $m_c(t)$, as described by Eq. (2). The values of D and $m_a(t)$, $m_b(t)$ and $m_c(t)$ are obtained from the control loops shown in Fig. 4 and described in Section 4.3. These are needed for a proper control of the power flow of the components of the MVDC microgrid.

$$V_{C1} = V_{MVDC} = \frac{1-D}{1-2D} \bullet \mathrm{V_{in}} \tag{1}$$

$$V_{dc} = \frac{1}{1-2D} \bullet \mathrm{V_{in}} = \mathrm{B} \bullet \mathrm{V_{in}}$$

$$v_a(t) = \frac{1}{\sqrt{3}} (V_{dc} \bullet \mathrm{m_a(t)})$$

$$v_b(t) = \frac{1}{\sqrt{3}} (V_{dc} \bullet \mathrm{m_b(t)})$$

$$v_c(t) = \frac{1}{\sqrt{3}} (V_{dc} \bullet \mathrm{m_c(t)}) \tag{2}$$

Now, substituting V_{dc} from Eq. (1) into Eq. (2), a direct relation can be obtained between the input voltage of the energy source (V_{in}) and the AC output voltage as in Eq. (3).

$$v_a(t) = \frac{B}{\sqrt{3}} (V_{in} \bullet \mathrm{m_a(t)})$$

$$v_b(t) = \frac{B}{\sqrt{3}} (V_{in} \bullet \mathrm{m_b(t)})$$

$$v_c(t) = \frac{B}{\sqrt{3}} (V_{in} \bullet \mathrm{m_c(t)}) \tag{3}$$

The voltage in the capacitor C2 (V_{C2}) can be obtained from V_{in}, as shown in Eq. (4). In the configuration of the charging station, this voltage also corresponds to the voltage of the BES (V_{BES})

$$V_{BES} = V_{in} \bullet \mathrm{B} \bullet \mathrm{D} \tag{4}$$

The value of the controlled current source is obtained based on the power balance principle ($P_{grid} + P_{dc} = P_{PV} + P_{BES}$) calculated in the PV side terminals (V_{in}).

$$P_{grid} = i_a(t) \bullet v_a(t) + i_b(t) \bullet v_b(t) + i_c(t) \bullet v_c(t)$$

$$P_{in} = V_{in} \bullet \mathrm{I_{in}}$$

$$P_{BES} = V_{C2} \bullet \mathrm{I_{BES}} = \mathrm{V_{BES}} \bullet \mathrm{I_{BES}}$$

$$P_{dc} = V_{dc} \bullet \mathrm{I_{dc}} = \mathrm{P_{PV}} - \mathrm{P_{H2}} \tag{5}$$

where P_{dc} is the input or output power in V_{dc}, which comes from the power of the hydrogen system and the EV.

Eq. (5) derived from the PV system side are the following, provided that the voltage in the BES is equivalent to $V_{in} \cdot B \cdot D$ [31].

$$P_{grid} = \frac{V_{in}}{\sqrt{3}} B (i_a(t) \cdot m_a(t) + i_b(t) \cdot m_b(t) + i_c(t) \cdot m_c(t))$$

$$P_{in} = V_{in} \bullet \mathrm{I_{in}}$$

$$P_{BES} = V_{in} \bullet \mathrm{B} \bullet \mathrm{D} \bullet \mathrm{I_{BES}}$$

$$P_{dc} = V_{in} \bullet \mathrm{B} \bullet \mathrm{I_{dc}} \tag{6}$$

Finally, if the power balance is carried out, the input current can be calculated.

$$I_{in} = \frac{B}{\sqrt{3}} (i_a(t) \bullet m_a(t) + i_b(t) \bullet m_b(t) + i_c(t) \bullet m_c(t)) - D \bullet \mathrm{B} \bullet \mathrm{I_{BES}} + \mathrm{B} \bullet \mathrm{I_{dc}} \tag{7}$$

where I_{in} is the current generated by the PV system (input current in the impedance network).

3.1.2. Averaged model of the DC/DC ZSC

Fig. 2b illustrates the averaged model of the DC/DC ZSC to which the hydrogen system and the EV charging units are connected. This model consists of a controlled current source in the input and a controlled voltage source at the output, and it is based on the converter designed in [29]. The converter reaches a high boost gain regulated with a duty cycle, making it more suitable and providing a good control for power regulation. The voltage gain of this converter is given by Eq. (8).

$$G = \frac{V_{out,ZSC}}{V_{in,ZSC}} = \frac{24.8 \bullet D_c - 0.8569 \bullet D_c^2}{0.0146 \bullet D_c + 0.3919} \tag{8}$$

In the configuration of the charging station, $V_{out,ZSC}$ corresponds to V_{MVDC} while $V_{in,\ ZSC}$ is related to the voltage of the EV batteries or the voltage of the hydrogen system (FC or LZ).

Finally, considering the power balance in the converter, the relation between the input and output current is obtained as follows.

$$G = \frac{I_{in,ZSC}}{I_{out,ZSC}} = \frac{V_{out,ZSC}}{V_{in,ZSC}} \tag{9}$$

3.2. Hydrogen system

As previously stated, the hydrogen system is composed of a FC, a LZ and a hydrogen tank. The LZ is responsible for generating hydrogen from water through electricity. The hydrogen produced is stored in the hydrogen tank. Then, the FC uses the stored hydrogen to produce electricity.

High power density, low operation temperature, high durability, high efficiency in comparison to internal combustion engine, and relatively good dynamic performance, are some features of FC [32–34]. For the present work, the FC modelling is based on the reduced model described in [35]. The main considerations and simplifications of this model are the following: 1) The incoming hydrogen and air are considered ideal gases; 2) the manifolds are not modeled, it is considered that the hydrogen comes directly from the tank, and the air from a compressor with stable mass flow; 3) the FC model does not use a humidifier nor an air-cooler, and thus, its relative humidity is constant and its working temperature is optimal.

The output voltage of the FC is given by Eq. (10). This voltage is calculated from the Nernsts instantaneous voltage (E_{cell}) and the irreversible voltage (V_{irrev}), which is obtained as the sum of two drop voltages V_{act} and V_{ohm}. In this paper, the concentration drop voltage is considered null.

$$V_{FC} = E_{cell} - V_{irrev} = E_{cell} - (V_{act} + V_{ohm}) \tag{10}$$

E_{cell} is calculated from Eq. (11).

$$E_{cell} = E_{cell}^0 - k_e(T - T_0) - \frac{RT}{2F} ln\left(\frac{p_{H20}}{p_{02}^{0.5} \bullet p_{H2}}\right) \tag{11}$$

On the other hand, among the different options available in the literature for LZ modelling, reduced linear models have proved sufficient accuracy for power dynamic studies, while maintaining lower complexity and computational effort than other detailed alternatives [36]. In general terms, the LZ is modeled in this work as a variable DC voltage source defined by Eq. (12). Pressure and temperature variations can affect the output voltage of the device (V_{LZ}), which is computed as a function of the reverse voltage (V_{rev}), the internal resistance of the LZ (R_i), and the instantaneous current (I_{LZ}) [37].

$$V_{LZ}(T,p) = V_{rev}(T,p) + I_{LZ}\bullet \mathrm{R_i(T,p)}) \tag{12}$$

It can be seen that the terms in Eq. (12) are temperature and pressure dependent, which makes this model applicable to studies where these magnitudes are susceptible of variation without the need to modify any other parameter of the model. Eq. (12) indicates that, under a given pressure and temperature, V_{LZ} shows a linear variation with I_{LZ}.

The reverse voltage is given by Eq. (13). This value has been chosen to replicate the polarization curve of a commercial LZ. Also, the reference pressure p_0 has been chosen with the same purpose. T and p stand for the LZ temperature and pressure, respectively.

$$V_{rev}(T,p) = V_{rev0} + \frac{RT}{2F} ln\left(\frac{p}{p_O}\right) \tag{13}$$

The LZ internal resistance is calculated through Eq. (14) Reference values are needed for the internal resistance (R_{i0}), pressure and temperature (T_0). The resistance variation with temperature and pressure is introduced through the coefficient dR_t and the factor k_{LZ}, respectively. These values have been taken from [37] and fine-tuned to reproduce the performance of the commercial LZ used as a reference in this work.

$$R_i(T,p) = R_{iO} + k_{LZ}\bullet \ln\left(\frac{\mathrm{p}}{\mathrm{p_O}}\right) + \mathrm{dR_i}\bullet(\mathrm{T} - \mathrm{T_o}) \tag{14}$$

Finally, the hydrogen level in the tank (L_{H2}) is obtained through Eq. (15).

$$L_{H2}(\%) = L_{H20}(\%) - 100\left(\frac{\int Q_{H2}\bullet dt}{CAP}\right) \tag{15}$$

3.3. Batteries models (BES and EV)

Currently, the most used battery technology for EV is based on Li-ion. The BES considered in this work is a lead-acid battery because it is one of the least expensive and presents a good capability [38].

These batteries are modelled based on the model available in the SimPowerSystems toolbox of Simulink [39], which has been adapted to properly represent the V-I and V-SOC curves and dynamic response of the device according to the information provided in the datasheets. The model consists of a variable voltage source and a series resistance.

$$V_{bat} = E_{bat} - I_{bat}\bullet \mathrm{R_{int}} \tag{16}$$

where E_{bat} depends on the charge or discharge of the battery, R_{int} is the internal resistance and I_{bat} is the battery current. Depending on the type of battery, the calculation of E_{bat} and R_{int} can differ.

Another important parameter of the battery is its state of charge (SOC), which needs to be controlled to avoid an over charge or a deep discharge. Eq. (17) determines the battery SOC

$$SOC(\%) = SOC_0(\%) - 100\left(\frac{\int I_{bat}\bullet dt}{Q}\right) \tag{17}$$

3.4. PV system

The model presented in [40] is used to implement the PV system, since it has already proved good accuracy and simplicity [41,42]. This model receives the irradiance and temperature as inputs, while the I-V characteristics are outputted. It is composed of a diode, a controlled current source, and two resistances (one in series and one in parallel). The output current of the PV system is given as follows.

$$I_{pv} = I_L - I_{sat}\left(e^{q\left(V_{pv}+I_{pv}R_s\right)/\left(NkT_{pv}\right)}\right) - \left(V_{pv} + I_{pv}R_s\right)/R_{sh} \tag{18}$$

$$I_L = L_{L0}\left(1 + K_0(T_{pv} - 300)\right)\frac{G_s}{G_n} \tag{19}$$

$$I_{sat} = K_1 T_{pv}^3 e^{-qV_g/kT_{pv}} \tag{20}$$

4. Energy management system (EMS) based on biogeography-based optimization (BBO)

In the microgrid, a proper energy management is crucial to use the energy sources efficiently and reduce the use of the local grid. In this sense, the terms 'equivalent hydrogen consumption and generation' form two important aspects to be considered in the energy management. Minimizing the equivalent hydrogen consumption and maximizing the equivalent hydrogen generation the ESS can be used longer (more efficiently), thus limiting the use of the grid only in certain situations. To achieve this objective, an EMS based on BBO is developed. BBO is used as an optimization algorithm to solve the objective function, and thereby, achieve the optimal operation point of the ESS. Note that if there is an excess of the energy from the PV system, the objective of the BBO is to maximize the equivalent hydrogen generation, whereas if there is a lack of energy to be injected to the EV, the objective is to minimize the equivalent hydrogen consumption. This lack or excess of energy is called net power (P_{NET}), which can be obtained as the difference between the power generated by the PV system and the power consumed by the EV.

$$P_{NET} = P_{PV} - P_{EV} \tag{21}$$

As it will be explained later, the EMS must discern between positive and negative values of this term.

Next sections illustrate the functions to be optimized, which are solved by BBO to achieve the optimization of the energy flow in the charging station. An introduction to BBO algorithm is also shown in this section.

4.1. Fitness function: equivalent hydrogen consumption and generation

In the microgrid, the hydrogen system and the BES can be used to generate or absorb energy (energy from P_{NET}).

If the BES supplies energy, the SOC decreases, and thus it will be recharged from the energy provided by the FC or the charging station in order to keep a desired SOC. In the event of a future lack of energy ($P_{NET} < 0$), an extra hydrogen consumption could be needed to produce the power demanded. If the BES is recharged, the SOC increases, and the BES will be used more often in future to provide energy, resulting in a saving of the hydrogen consumption. Due to this fact, when a new energy surplus occurs ($P_{NET} > 0$), the electrical energy consumption in the BES is transformed into equivalent hydrogen.

The equivalent hydrogen consumption is composed of the sum of the FC hydrogen consumption and the equivalent hydrogen consumption of the BES.

$$Q_{H2,con}^{eq} = Q_{H2,FC} + KQ_{BES,con} \tag{22}$$

The hydrogen consumption of the FC is given by Eq. (23), where η_{FC} is approximated by the fourth order polynomial shown in Eq. (24).

$$Q_{H2,FC} = \frac{P_{FC}}{PCI_{H2}\bullet\eta_{ther}\bullet U_f\bullet\eta_{FC}} \tag{23}$$

$$\eta_{FC} = P_1\cdot P_{FC}^4 + P_2\cdot P_{FC}^3 + P_3\cdot P_{FC}^2 + P_4\cdot P_{FC} + P_5 \tag{24}$$

Eqs. (25)–(27) show the expression used to obtain the equivalent hydrogen consumption of the BES.

$$Q_{BES,con} = \frac{P_{BES}\bullet Q_{H2,FC}^{avg}}{P_{FC}^{avg}\bullet\eta_{dis}\bullet\eta_{char}^{avg}} \tag{25}$$

$$\eta_{dis} = 0.5\left(1 + \sqrt{1 - \frac{4\bullet R_{BES}\bullet P_{BES}}{U_{BES}^2}}\right) \tag{26}$$

$$K = 1 - 2\mu_{SOC}\frac{[SOC - 0.5(SOC_{max} + SOC_{min})]}{SOC_{max} + SOC_{min}} \tag{27}$$

As described in [43], the equivalent hydrogen consumption depends on the power and SOC of the BES. Besides, since the future operating points of the FC and BES are unknown, the average hydrogen consumption of the FC ($Q_{H2,FC}^{avg}$) and the average FC power are needed (P_{FC}^{avg}). The term K is a penalty coefficient used to change the equivalent hydrogen consumption of the BES according to the deviation of the SOC from the desirable value. The charging and discharging performance of the BES can be introduced by adjusting μ_{SOC}, which presents a value of 0.6 in this work [44].

On the other hand, the equivalent hydrogen generation is calculated as the sum of the hydrogen generation of the LZ and the equivalent hydrogen generation of the BES.

$$Q_{H2,gen}^{eq} = Q_{H2,LZ} + KQ_{BES,gen} \tag{28}$$

Eqs. (29) and (30) show the expressions used to calculate the hydrogen generation of the LZ. As in the case of the FC, the LZ efficiency (η_{LZ}) is approximated by a fourth order polynomial.

$$Q_{H2,LZ} = max\left(\frac{|P_{LZ}| - B \bullet q_{H2,LZ}^{nom}}{PCS_{H2}/\eta_{LZ}}, 0\right) \tag{29}$$

$$\eta_{LZ} = P_1 \cdot P_{LZ}^4 + P_2 \cdot P_{LZ}^3 + P_3 \cdot P_{LZ}^2 + P_4 \cdot P_{LZ} + P_5 \tag{30}$$

Regarding the equivalent hydrogen generation of the BES, analogue expressions to the equivalent hydrogen consumption are used.

$$Q_{BES,gen} = \frac{|P_{BES}| \bullet Q_{H2,LZ}^{avg}}{P_{LZ}^{avg} \bullet \eta_{char} \bullet} \eta_{dis}^{avg} \tag{31}$$

$$\eta_{char} = 2/\left(1 + \sqrt{1 - \frac{4 \bullet R_{BES} \bullet P_{BES}}{U_{BES}^2}}\right) \tag{32}$$

Next sections develop the fitness functions to be optimized by the BBO. In this algorithm, the habitat suitability index (HSI) is equivalent to the fitness function. This term is explained in section 4.2.

4.1.1. Equivalent hydrogen consumption minimization

A positive P_{NET} means that the BES or the FC have to generate extra power to provide the power demanded by the EV. In this case, the fitness function tries to minimise the equivalent hydrogen consumption given by Eq. (22), which includes a penalization (third term) associated to the use of the grid or the non-compliance with the first restriction (Eq. (34)). The penalization corresponds to the maximum value between $Q_{H2,FC}$ and $K \bullet Q_{BAT,con}$.

$$HSI = min\left(Q_{H2,FC} + K \bullet Q_{BES,con} + \max\left(Q_{H2,FC}, K \bullet Q_{BES,con}\right)\big|_{Pgrid}\right) \tag{33}$$

Subject to

$$P_{BES} + P_{FC} = P_{NET} \tag{34}$$

$$P_{BES} \le min\left(\frac{U_{BAT}^{min}\left(U_{BES} - U_{BES}^{min}\right)}{R_{BES}}, P_{BES}^{max}\right) \tag{35}$$

$$P_{FC} \le P_{FC}^{max}; \left[\begin{array}{c} P_{FC}^{max} = \frac{L_{H2}}{L_{H2}^{min}} P_{FC}^{nom} conL_{H2} \le L_{H2}^{min}(10\%) \\ P_{FC}^{max} = P_{FC}^{nom} conL_{H2} > L_{H2}^{min}(10\%) \end{array}\right] \tag{36}$$

The first restriction (Eq. (34)) makes the power balance among the components of the charging station possible. The second (Eq. (35)) and the third (Eq. (36)) restrictions limit the power to be generated by the BES and the FC, according to the BES SOC and the level of hydrogen in the tank. Note that, in the case of the BES, the SOC depends on the BES output voltage; and in the case of the FC, the level of hydrogen must be known.

4.1.2. Equivalent hydrogen generation maximization

When P_{NET} is negative, the BES or the LZ have to absorb the surplus power from the PV system not used by the EV. In this case, the fitness function tries to maximize the equivalent hydrogen generation given by Eq. (28). Again, a third term associated to the use of the grid is included. The non-compliance whit the first restriction is penalized as the minimum value between $Q_{H2,LZ}$ and $K \bullet Q_{BAT,gen}$.

$$HSI = max\left(Q_{H2,LZ} + K \bullet Q_{BES,gen} - \min\left(Q_{H2,LZ}, K \bullet Q_{BES,gen}\right)\big|_{Pgrid}\right) \tag{37}$$

Subject to:

$$P_{BES} + P_{LZ} = P_{NET} \tag{38}$$

$$P_{BES} \le -1 \bullet \min\left(\frac{U_{BES}^{max}\left(U_{BES}^{max} - U_{BAT}\right)}{R_{BES}}, P_{BES}^{max}\right) \tag{39}$$

$$P_{LZ} \le -1 \bullet P_{LZ}^{max}; \left[\begin{array}{c} P_{LZ}^{max} = \frac{100 - L_{H2}}{100 - L_{H2}^{max}} P_{LZ}^{nom} conL_{H2} \ge L_{H2}^{max}(95\%) \\ P_{LZ}^{max} = P_{LZ}^{nom} conL_{H2} < L_{H2}^{max}(95\%) \end{array}\right] \tag{40}$$

In this case, the maximization problem is also restricted by the power balance, Eq. (37), and the maximum power that the BES and LZ can absorb, Eqs. (39) and (40), respectively.

4.2. Biogeography-based optimization (BBO)

Nowadays, as it occurred with other intelligent techniques such as genetic algorithms (GA), particle swarm optimization (PSO), or fuzzy logic; biogeography is starting to be applied to solve engineering problems. There are two important definitions in biogeography: habitat suitability index (HSI) and suitability index variables (SIV).

A high HSI implies that many species can emigrate to nearby habitats, and a low immigration rate, since the habitat is already saturated. Otherwise, SIV represents the terms that describe the habitability of a habitat. In an optimization problem, HSI is the dependent variable and SIV is the independent variable.

Fig. 3 shows the typical immigration and emigration curves of a habitat with a maximum number of species S_{max} (see curves at straight line). λ and μ are, respectively, the immigration and emigration rates. If there is no species in the habitat, the maximum immigration rate I is obtained. Similarly, the maximum emigration rate E, occurs if the

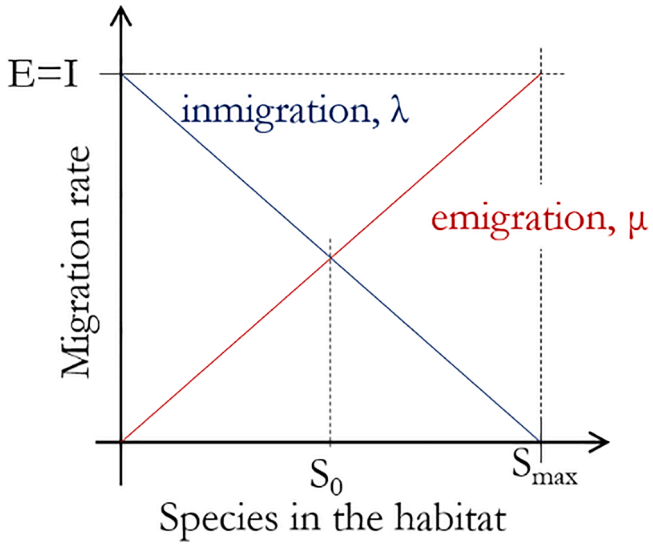

Fig. 3. Model of species for a single habitat [19].

habitat is supporting S_{max} species on it. S_o is the number of species that gets the equilibrium between λ and μ.

In BBO, a feasible solution is represented by an island composed of a real number of SIV. The suitability of an island is calculated as the measure of the HSI.

$$HSI = f(SIV_1, SIV_2, \cdots SIV_n) \tag{41}$$

High values of HSI are better solutions that low ones. Therefore, the aim of BBO is to maximize HSI considering all the SIV. The following equations can be given for the K[th] species from Fig. 3. Note that if $E = I$, both rates are related as $\mu_K + \lambda_K = 1$ [19].

$$\mu_K = E\left(\frac{K}{n}\right)$$

$$\lambda_K = I\left(1 - \frac{K}{n}\right) \tag{42}$$

where n is defined as S_{max}.

The probability that a habitat contains certain number of species, S, is expressed as follows.

$$P_S(t + \Delta t) = P_S(t)(1 - \lambda_s \Delta t - \mu_s \Delta t) + P_{S-1}(t)\lambda_{s-1}\Delta t + P_{S+1}(t)\mu_{s+1}\Delta t \tag{43}$$

The first term of Eq. (43) represents the probability of S species at time t and with no migration, the second term is the probability of S-1 species at time t and one immigration, and the third term is the probability of $S + 1$ species at time t and one emigration.

In BBO, as in other algorithms, a vector of SIV represents a population of candidate solutions. The exchange of information among the habitats is related through the migration rates (μ and λ), which are controlled by the island modification probability.

In biogeography, abrupt changes in the HSI can modify a certain habitat. BBO simulates this effect as mutation rates, which are obtained using species count probabilities. The likelihood that a certain number of species (P_s) exist is necessary in the probabilistic operator to know the mutation probability. Solutions with low P_s will tend to mutate to other solution. On the contrary, high P_s solution are less likely to mutate. This fact can be modelled by the mutation rate using the following equation.

$$m(S) = m_{max}\left(\frac{1 - P_s}{P_{max}}\right) \tag{44}$$

where m_{max} is defined by the user.

A synthesis of the BBO algorithm is illustrated as follows: a) define the BBO parameters, such as S_{max}, E, I and m_{max}; b) initialize a random set of solutions to the problem and calculate HSI for each solution; c) for each habitat, calculate S, λ, and μ; d) modify habitats (migration) based on λ, μ, and then, mutation based on probability; e) go to step b) for the next iteration if needed, and if not, SIV with highest HSI is the final solution.

4.3. Control loops

Fig. 4 shows the control loops implemented to manage the reference powers generated by the EMS based on BBO, denoted as BBO-EMS (Fig. 4a), to generate the MPPT power for the PV system (Fig. 4b), and to charge the BES of the EV (Fig. 4c).

It can be observed in Fig. 4a that the BES power is controlled by means of the shoot-through period of the qZSI. This term is calculated as the sum of other two terms in order to achieve a fast response of the

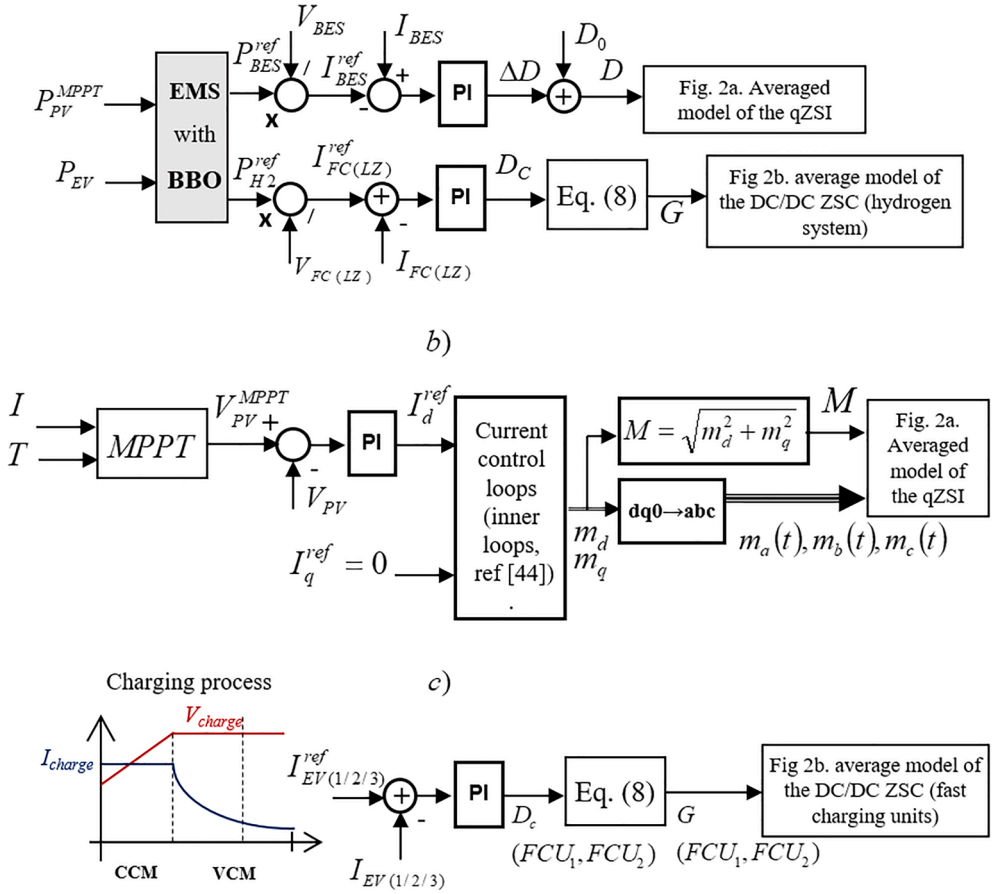

Fig. 4. Control schemes implemented for the ZSC: a) qZSI (battery control) and DC/DC ZSC for the hydrogen system (FC and LZ), b) qZSI (active and reactive power), and c) DC/DC ZSC for the fast-charging units.

system.

$$D = \Delta D + D_o \tag{45}$$

where ΔD is the output of the BES current control loop, and D_0 is defined by Eq. (46).

D_o relates the input voltage of the qZSI (V_{PV}^{MPPT}) with the nominal voltage across the capacitor C_2 (nominal voltage of the BES, V_{BES}^{nom}). Note that, for a certain irradiance, D_0 is a constant term. Therefore, ΔD moves around D_o with the aim of controlling the desirable variable.

$$D_0 = V_{BES}^{nom} / \left(2 \bullet V_{\mathrm{BES}}^{\mathrm{nom}} + V_{\mathrm{PV}}^{\mathrm{MPPT}}\right) \tag{46}$$

Moreover, the hydrogen system power (FC or LZ power) is controlled through the duty cycle of the DC/DC ZSC. If D_c is known, the boost factor of the converter can be calculated (Eq. (8)) and therefore control the hydrogen system power.

The three-phase modulating signals ($m_a(t)$, $m_b(t)$ and $m_c(t)$), and thus M, are controlled to regulate the active power generated by the PV system and injected into the grid through the qZSI, as shown in Fig. 4b. The reference value for I_d^{ref} is provided by a PI controller in the outer control loop. This controller is in charge of maximizing the power generated by the PV system by acting on the PV generation voltage (MPPT). The reactive power has been set to zero ($I_q^{ref} = 0$). The inner loops are the current control loops, where two PI controllers regulate the d and q components of the grid current by means of the d and q components of $v_a(t)$, $v_b(t)$ and $v_c(t)$. A detailed description of these loops can be found in [45].

Fig. 4c illustrates that the current needed to charge the BES of the EVs is controlled through the duty cycle of the DC/DC ZSC (similar control to that used in the hydrogen system).

The charging process of the EVs considered in this work is based on two modes or stages, called constant current mode (CCM) and constant voltage mode (CVM). Once the EV is connected to the fast-charging unit, the charging process starts in the CCM, in which the EV is charged with a constant current (previously imposed depending on the type of BES) and the voltage of the EV increases gradually. The process switches to the CVM, when the BES reaches its nominal charge voltage. In this mode, the EV is charged keeping the voltage constant, and therefore, the charging current gradually decreases. The charging process is finished when the current is lower than a 5% of the charging current for a pre-set time (5 min).

5. Results and discussion

This section has two objectives. On the one hand, it clarifies the selection of the values of the main parameters of the BBO and demonstrates the output values of the HSI are correct (Section 5.1). On the other hand, it shows the performance and technical viability of the BBO-EMS applied on the microgrid described in Section 2, and assesses the suitability of using ZSC for this kind of application (Section 5.2).

Furthermore, the EMS presented in this work is compared with a simpler EMS already developed in [46]. In [46], the EMS was applied to a hybrid system with two renewable energy sources, a BES, a hydrogen system and a AC load connected through an inverter. It was adapted to the configuration of the MVDC microgrid under study in this work . Both EMS are assessed to quantify how good the proposed EMS is when compared with one previously applied to a similar microgrid. The EMS used in [46] determinates the reference power for the hydrogen system and BES proportionally to the hydrogen tank level and the BES SOC, achieving a very effective control of these parameters (L_{H2} and SOC). This EMS tries to optimize the energy available in the hydrogen tank and BES but without considering the total equivalent hydrogen consumption and generation. The comparison is carried out through a 1200 s simulation under different conditions of sun irradiance and considering the connection of several EVs to the charging station. In the study, the proposed EMS is denoted as BBO-EMS and the EMS based on [46] as PRO-EMS (proportional EMS).

The configuration of the MVDC microgrid used for the comparison has been included in Section 2. The PV system has a peak power of 186 kW, which is reached with a 55x16 panel structure. The BES has a rated capacity of 76.45 kWh and a rated power of 180 kW. The hydrogen system is composed of six FC with a peak power of 66 kW, a 176 kVA electrolyzer and a 450 kg metal hydrogen tank. The MVDC microgrid has two fast charging units (EV charging mode 4) with a rated power of 48 kW each. Finally, the power of the grid is limited to 100 kVA in both directions (rated power of a typical transformer), although, as it will be shown, this value is never reached. The rated power of the system has been set to 186 kW (peak power of the PV system). Hence, the per unit values shown in the figures of this section were obtained from this value.

5.1. BBO selection of parameters

The value of the main parameters of the BBO, such as, "mutation probability", "number of iterations", "population size" and "number of elites", were selected after carrying out a sensitivity analysis based on the Monte Carlo Simulation. For this simulation, a scenario of 50 s was created. The EMS based on BBO was implemented for each possible combination of "mutation probability", "number of iterations", "population size" and "number of elites", and finally, the sum of HSI (Eq. (33)) was evaluated. In this sensitivity analysis, the range of values considered for each parameter were the following: "mutation probability" [0.02, 0.04, 0.06, 0.08]; "number of iterations" [5, 15, 25, 35, 45, 55, 65, 75, 85, 95]; "population size" [10, 20, 30] and "number of elites" [1, 2, 3, 4]. The results of this simulation reflect (after 480 feasible combinations), that only the number of iterations affects the final value of the sum of HSI. Table 1 and Fig. 5a show the sum of HSI (in pu) versus the maximum number of iterations with fixed values of "population size", "mutation probability", "number of elites" that minimizes the computational effort. It can be observed that from 75 iterations on the sum of HSI reaches the same value. It can be understood that the best value of the HSI has been achieved. Therefore, the final combination of parameters considered for the simulation showed in the next section was: "mutation probability" =0.02; "population size" =10; "number of elites" =1 and "maximum number of iterations" =75.

Finally, Fig. 5b shows the error of the HSI (defined as the best value in one iteration minus the best value of the previous iteration) versus the iterations for the selected combination of parameters. This subplot represents the first four times that the BBO is executed in the simulation carried out in Section 5.2. It can be observed that the error converges to zero as the 75 iterations are completed, when the optimum value of the HSI is reached. According to the previous results, it can be concluded that the BBO parameters selected are correct and that the BBO-EMS works properly.

5.2. Technical viability of the BBO-EMS

Fig. 6a depicts, in per unit, the power demanded by each EV and the

Table 1
Summary of Monte Carlo Simulation.

Maximum number of iterations	Sum of HSI. Eq. (33), pu	Population size	Mutation probability	Number of elites
5	1,17	10	0,02	1
15	1,12	10	0,02	1
25	1,10	10	0,02	1
35	1,07	10	0,02	1
45	1,07	10	0,02	1
55	1,02	10	0,02	1
65	1,02	10	0,02	1
75	1,00	10	0,02	1
85	1,00	10	0,02	1
95	1,00	10	0,02	1

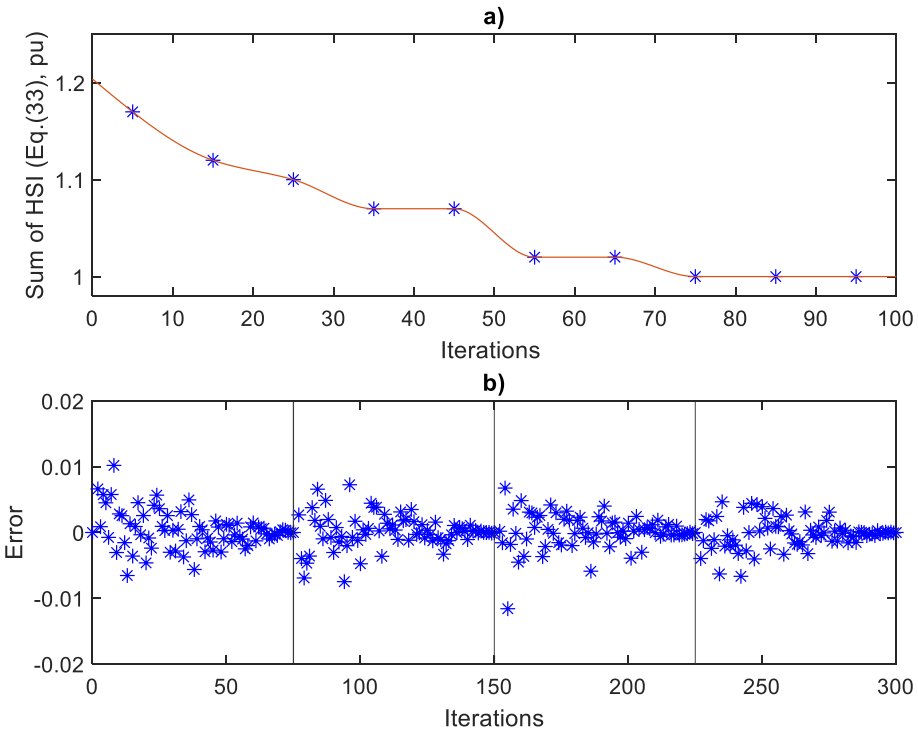

Fig. 5. a) Sum of HSI vs maximum number of iterations, and b) error of HSI vs iterations.

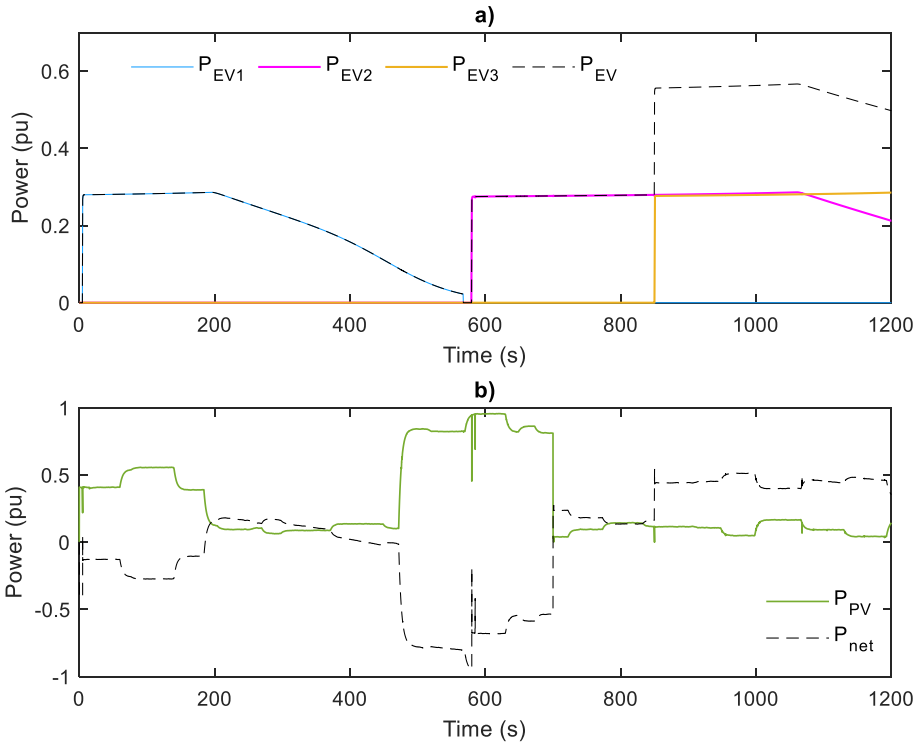

Fig. 6. a) Power demanded by the EV, and b) PV system power and net power.

total power required by the charging station (sum of the EVs). This charging power corresponds to a fast charge of the EVs, and thus, the nominal power is 48 kW. The first EV is charged from 2 s to 570 s, the second EV is connected at 580 s, and the third EV at 580 s. The SOC of the BES of these EV are shown in Fig. 8b and 8c. Note that, although there are two fast-charging units, three EV are considered. The first and the third EV are connected to a fast-charging unit, and the second EV to the other one.

The power generated by the PV system is depicted in Fig. 6b. It also shows the net power, P_{NET}, difference between the PV power and the total power demanded by the EV (black dotted-line in Fig. 6b). These parameters are inputs of the EMS. Positive values correspond to power to be generated by the hydrogen system (minimizing equivalent hydrogen consumption), while negative values represent power to be

absorbed (maximizing equivalent hydrogen generation). The maximum power generated by the PV system is almost 1p.u. (at 600 s), which is approximately the rated power of the MVDC microgrid. This peak power is injected into the system, and if there were no EV connected, the BES or the hydrogen system would have to absorb this power.

Fig. 7a represents the powers of the hydrogen system (FC and LZ), BES and grid with the BBO-EMS. It can be observed that the grid is used to control the voltage of the system generating (absorbing) those peaks of power that neither the hydrogen system nor the BES are able to generate (absorb), as illustrated in seconds 580 and 850 approximately. The power balance is mainly controlled by the EMS. The P_{NET} with both EMS (BBO-EMS and PRO-EMS) is represented in Fig. 7b. In both cases, the tracking of this power is quite accurate, which verifies that both EMS can be applied to the microgrid under study. Nevertheless, around the second 580 and at the end of the simulation, the PRO-EMS cannot follow appropriately the dynamic of P_{NET}. This fact penalizes the equivalent hydrogen consumption and generation (Fig. 8a).

The equivalent hydrogen flow (consumption and generation) with both EMS is illustrated in Fig. 7a. Negative values are associated to the generation of equivalent hydrogen flow (negative value of P_{net}), and thus, the more negative the value, the more hydrogen is generated. On the contrary, the consumption of the equivalent hydrogen is associated to positive values of P_{net}. Throughout the simulation, it can be seen that, with the BBO-EMS, lower hydrogen consumption and higher hydrogen generation is achieved when compared to the PRO-EMS. The final values of the equivalent hydrogen generation and consumption are provided in Table 2. Moreover, the BES SOC, the hydrogen tank level and the EV battery SOC are shown in Fig. 8b (BBO-EMS) and Fig. 8c (PRO-EMS). As expected, the EV battery SOC have the same values with both EMS, since the power demanded by these batteries during their charge is considered an input of the system regardless of the EMS. On the contrary, the BES SOC and the hydrogen tank level depend on the EMS. Although they follow the same trend, it can be observed that with the PRO-EMS the hydrogen tank level becomes low before the BES SOC. Thus, during the last 100 s of the simulation, the BES has to generate all the power demanded, and the equivalent hydrogen consumption is significantly higher than with the BBO-EMS.

Finally, Fig. 9 shows the main voltages of the microgrid station and the switching indexes obtained with the BBO-EMS. The BES and PV voltage, and V_{MVDC} are illustrated in Fig. 9a. The voltage of the EV battery and the hydrogen system voltage are represented in Fig. 9b. In these figures, V_{H2} denotes the combination of the LZ and FC voltage. For negative values of the net power, V_{H2} corresponds to the LZ voltage (the FC is disconnected) and, for positive values, V_{H2} corresponds to the LZ voltage (the LZ is disconnected). The switching indexes of the qZSI, D and M (shoot-through duty cycle and index modulation) are depicted in Fig. 9c. Moreover, Fig. 9d shows the duty cycle of the DC/DC ZSC, (Eq. (8)). Note that, although there are two fast charging units (two converters), three EVs are connected to the charging station. A value of zero in these indexes imply the lack of an EV connected to the converter. If the D of the converter of the hydrogen system is zero, it means that neither the LZ or the FC are connected.

Table 2 shows the final results corresponding to the total consumption and generation of hydrogen (in kg) with both EMS. The sum of the HSI, the total equivalent hydrogen consumption and generation ($M^{eq}_{H2,con}$, $M^{eq}_{H2,gen}$) and the total hydrogen generation and consumption ($M^{eq}_{H2,con}$, $M^{eq}_{H2,gen}$) are provided. Note that the difference between the sum of HSI and $M^{eq}_{H2,con}$ ($M^{eq}_{H2,gen}$) resides in the penalization term. According to these results, it can be stated that the BBO-EMS is perfectly valid for this kind of application. Moreover, as it was expected, comparing the sum of HSI and $M^{eq}_{H2,con}/M^{eq}_{H2,gen}$ in both EMS, it can be seen that the BBO-EMS achieves quite better results, since the BBO algorithm optimizes these parameters to manage the energy of the microgrid. Hence, the sum of HSI and $M^{eq}_{H2,con}$ are 33.6% and 16.4% lower respectively compared to the PRO-EMS. Similarly, the sum of HSI and $M^{eq}_{H2,gen}$ are almost twice as much in comparison with the PRO-EMS. On the other hand, the results illustrate that, with the BBO-EMS, the hydrogen consumption ($Q_{H2,FC}$) is almost 40% lower that with the PRO-EMS. This fact also affects to the hydrogen generation ($Q_{H2,LZ}$), since the electrolyser has to produce less

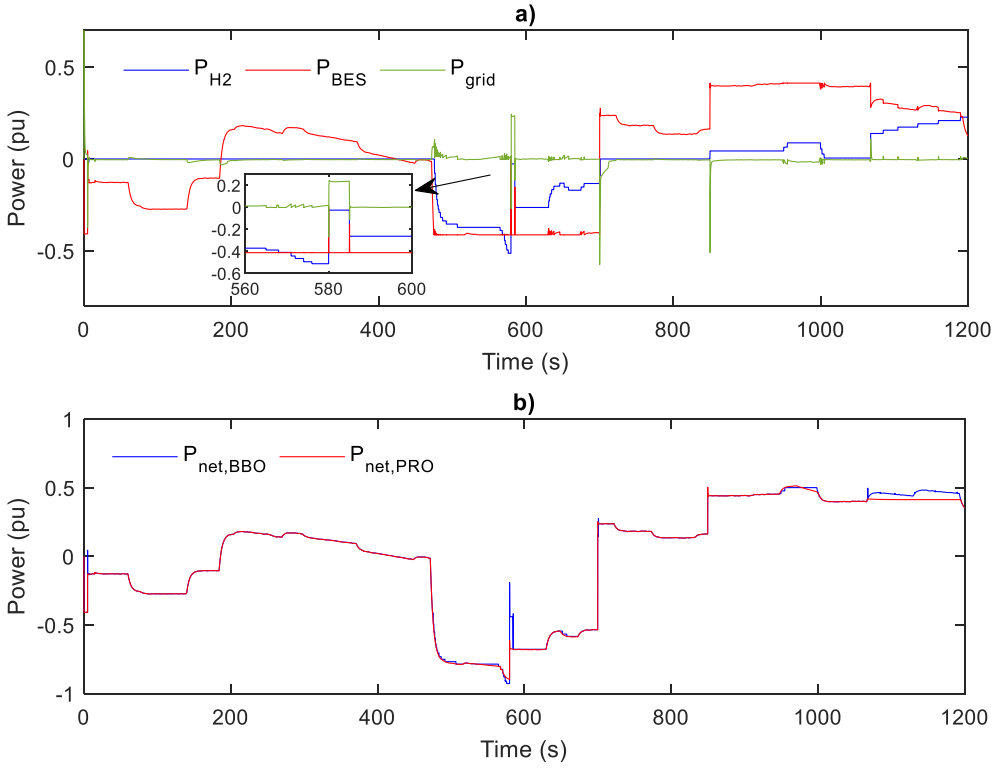

Fig. 7. a) Hydrogen system (H2), BES and grid power with BBO-EMS, and b) Net power generated with both EMS.

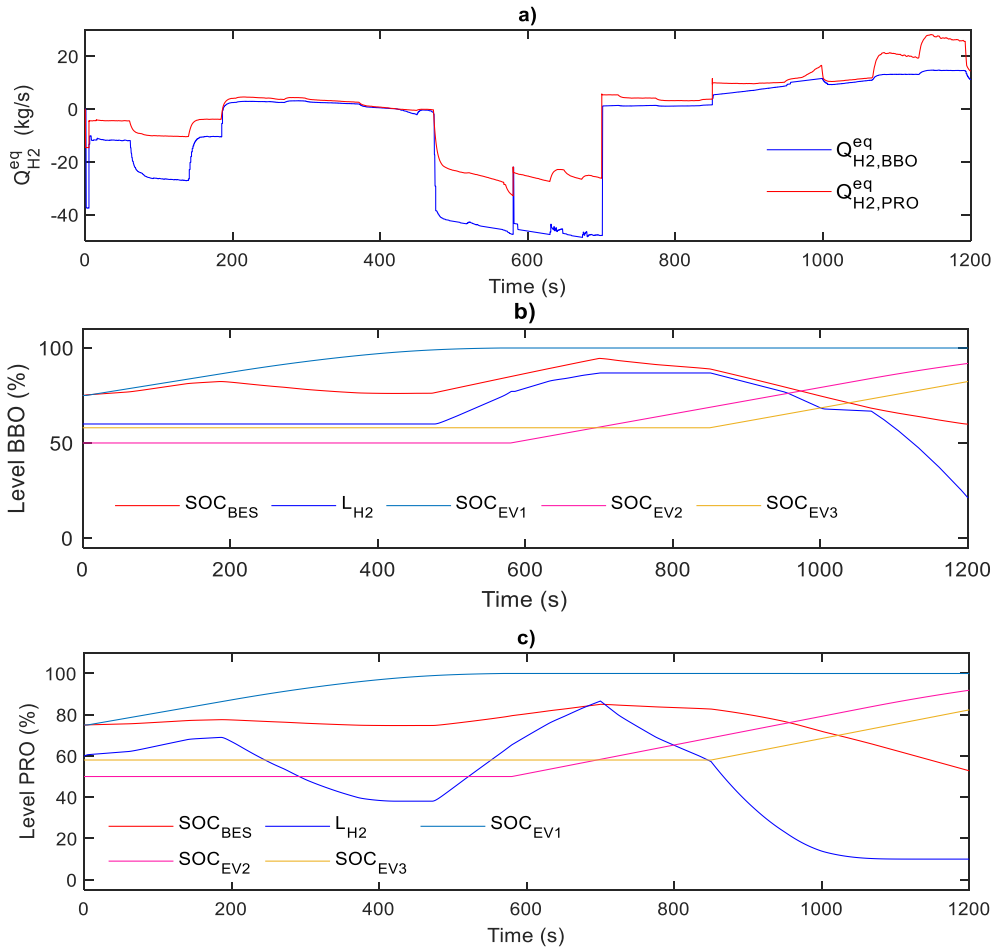

Fig. 8. a) Equivalent hydrogen flow with both EMS, b) BES SOC, hydrogen tank level and EV battery SOC with the BBO-EMS, and c) BES SOC, hydrogen tank level and EV battery SOC with the PRO-EMS.

Table 2
Total consumption and generation of hydrogen with both EMS.

		BBO-EMS	PRO-EMS
Consumption [kg]	Sum of *HSI* (Eq. (33))	4.463 (−33.6%)	6.725
	$M^{eq}_{H2,con}$ (sum of $Q^{eq}_{H2,con}$, section 4.1.1)	4.392 (−16.4%)	5.525
	$M_{H2,FC}$ (sum of $Q_{H2,FC}$, Eq. (23))	1.969 (−38.9%)	3.224
Generation [kg]	Sum of *HSI* (Eq. (37))	13.556 (+94,3%)	6.982
	$M^{eq}_{H2,gen}$ (sum of $Q^{eq}_{H2,gen}$ section 4.1.2)	13.690 (+95.5%)	7.001
	$M_{H2,LZ}$ (sum of $Q_{H2,LZ}$, Eq. (29))	1.373 (−43.2%)	2.414

hydrogen to supply the demand from the FC (−43.2%).

6. Conclusions

This paper presented an EMS based on a BBO algorithm applied to a microgrid that integrates a novel configuration with ZSC. The main contributions of this work were: 1) the design of a EMS based on BBO, which considers the concept of equivalent hydrogen, and therefore, optimizes the generation and consumption of equivalent hydrogen in the microgrid; 2) the development of a microgrid composed of a PV system, BES, a complete hydrogen system (FC, LZ and hydrogen tank), a local grid connection, and two fast charging units for EV, which are connected to each other by means of a configuration that integrates ZSC and MVDC. Additionally, the EMS was compared with a simpler EMS already applied on a similar configuration of hybrid system. The simulation results showed that the new configuration based on ZSC is perfectly valid for this application, since several conventional DC/DC converters were saved. Furthermore, it was proven along the simulation (performance under several conditions of sun irradiance and the connection of three EV) that, although both EMS can be used in the charging station, the EMS based on BBO achieved better results in the equivalent hydrogen consumption and generation, which implied a less dependence on the local grid.

CRediT authorship contribution statement

Lais de Oliveira-Assis: Conceptualization, Formal analysis, Investigation, Methodology, Writing – original draft. **Pablo García-Triviño:** Conceptualization, Formal analysis, Investigation, Methodology, Writing – original draft. **Emanuel P.P. Soares-Ramos:** Conceptualization, Formal analysis, Investigation, Methodology, Writing – original draft. **Raúl Sarrias-Mena:** Conceptualization, Formal analysis, Investigation, Methodology, Writing – original draft. **Carlos Andrés García-Vázquez:** Conceptualization, Formal analysis, Investigation, Methodology, Writing – original draft. **Carlos Ernesto Ugalde-Loo:** Conceptualization, Formal analysis, Investigation, Methodology, Writing – review & editing. **Luis M. Fernández-Ramírez:** Conceptualization, Funding acquisition, Methodology, Project administration, Supervision, Writing – review & editing.

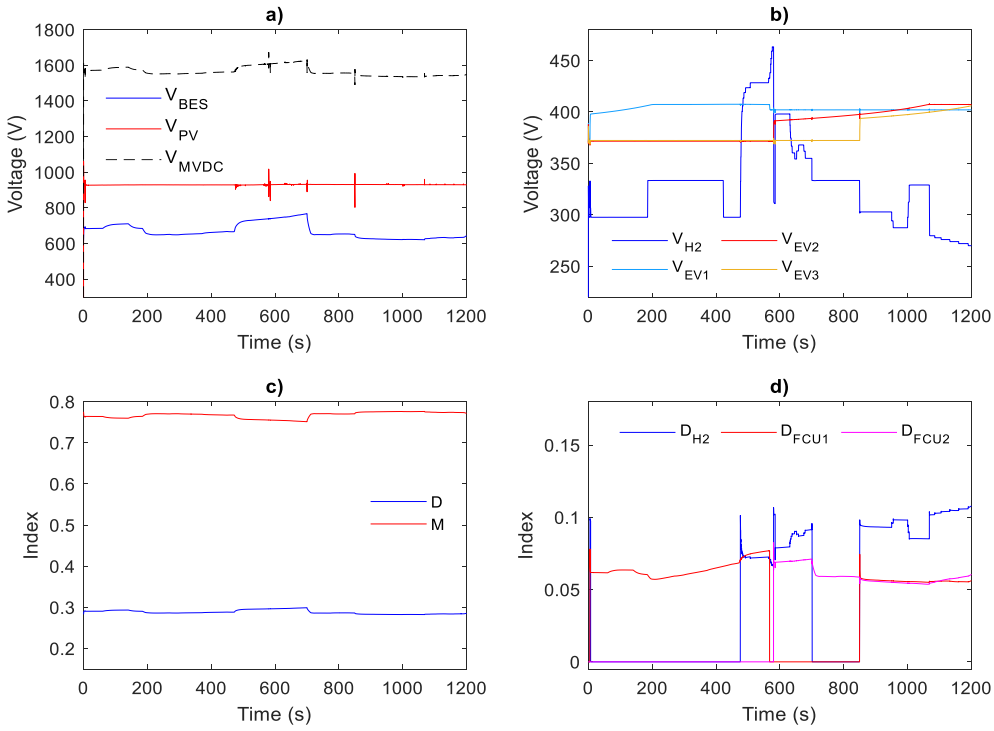

Fig. 9. a) Voltages of BES, PV system and MVDC bus, b) voltages of the hydrogen system and EV battery, c) *D* and *M* indexes of the qZSI, and d) duty cycles of the ZSC.

Declaration of Competing Interest

The authors declare that they have no known competing financial interests or personal relationships that could have appeared to influence the work reported in this paper.

Acknowledgments

This work was partially supported by Spain's Ministerio de Ciencia, Innovación y Universidades (MCIU), Agencia Estatal de Investigación (AEI) and Fondo Europeo de Desarrollo Regional (FEDER) Unión Europea (UE) (grant number RTI2018-095720-B-C32), by the Federal Center for Technological Education of Minas Gerais, Brazil (process number 23062-010087/2017-51) and by the National Council of Technological and Scientific Development (CNPq-Brazil).

References

[1] Farrokhabadi M, Canizares CA, Simpson-Porco JW, Nasr E, Fan L, Mendoza-Araya PA, et al. Microgrid stability definitions, analysis, and examples. IEEE Trans Power Syst 2020;35(1):13–29. https://doi.org/10.1109/TPWRS.2019.2925703.

[2] Rahman MM, Oni AO, Gemechu E, Kumar A. Assessment of energy storage technologies: a review. Energy Convers Manag 2020;223:113295. https://doi.org/10.1016/j.enconman.2020.113295.

[3] García-Triviño P, Fernández-Ramírez LM, Gil-Mena AJ, Llorens-Iborra F, García-Vázquez CA, Jurado F. Optimized operation combining costs, efficiency and lifetime of a hybrid renewable energy system with energy storage by battery and hydrogen in grid-connected applications. Int J Hydrogen Energy 2016;41(48):23132–44. https://doi.org/10.1016/j.ijhydene.2016.09.140.

[4] May GJ, Davidson A, Monahov B. Lead batteries for utility energy storage: a review. J Energy Storage 2018;15:145–57. https://doi.org/10.1016/j.est.2017.11.008.

[5] García-Triviño P, Gil-Mena AJ, Llorens-Iborra F, García-Vázquez CA, Fernández-Ramírez LM, Jurado F. Power control based on particle swarm optimization of grid-connected inverter for hybrid renewable energy system. Energy Convers Manag 2015;91:83–92. https://doi.org/10.1016/j.enconman.2014.11.051.

[6] García P, Torreglosa JP, Fernández LM, Jurado F, Langella R, Testa A. Energy management system based on techno-economic optimization for microgrids. Electr Power Syst Res 2016;131(1):49–59. https://doi.org/10.1016/j.epsr.2015.09.017.

[7] European Commission EC. Communication COM/2020/301: A hydrogen strategy for a climate-neutral Europe. Available from: https://eur-lex.europa.eu/legal-content/EN/TXT/PDF/?uri=CELEX:52020DC0301&from=EN. 2020 [accessed July 2020].

[8] International Renewable Energy Agency Green Hydrogen. A guide to policy making. Available from: < https://www.irena.org/-/media/Files/IRENA/Agency/Publication/2020/Nov/IRENA_Green_hydrogen_policy_2020.pdf> [accessed September 2020].

[9] International Renewable Energy Agency Green hydrogen. Green Hydrogen Cost Reduction: Scaling up Electrolysers to Meet the 1.50C Climate Goal. Available from: < https://www.irena.org/-/media/Files/IRENA/Agency/Publication/2020/Dec/IRENA_Green_hydrogen_cost_2020.pdf> [accessed September 2020].

[10] Das HS, Rahman MM, Li S, Tan CW. Electric vehicles standards, charging infrastructure, and impact on grid integration: a technological review Society of Automotive Engineers. Renew Sustain Energy Rev 2020;120:109618. https://doi.org/10.1016/j.rser.2019.109618.

[11] Dragicevic T, Lu X, Vasquez JC, Guerrero JM. DC microgrids – Part II: a review of power architectures, applications, and standardization issues. IEEE Trans Power Electron 2016;31(5):3528–49. https://doi.org/10.1109/TPEL.2015.2464277.

[12] Ullah S, Haidar AMA, Hoole P, Zen H, Ahfock T. The current state of Distributed Renewable Generation, challenges of interconnection and opportunities for energy conversion based DC microgrids. J Clean Prod 2020;273:122777. https://doi.org/10.1016/j.jclepro.2020.122777.

[13] Tulpule PJ, Marano V, Yurkovich S, Rizzoni G. Economic and environmental impacts of a PV powered workplace parking garage charging station. Appl Energy 2013;108:323–32. https://doi.org/10.1016/j.apenergy.2013.02.068.

[14] Domínguez-Navarro JA, Dufo-López R, Yusta-Loyo JM, Artal-Sevil JS, Bernal-Agustín JL. Design of an electric vehicle fast-charging station with integration of renewable energy and storage systems. Int J Electr Power Energy Syst 2019;105:46–58. https://doi.org/10.1016/j.ijepes.2018.08.001.

[15] Eissa M. Medium voltage direct current grid: resilient operation, control and protection. 1st ed. Amsterdan: Amsterdam Elsevier Academic Press; 2019.

[16] Pires VF, Romero-cadaval E, Vinnikov D, Roasto I, Martins JF. Power converter interfaces for electrochemical energy storage systems – a review. Energy Convers Manag 2014;86:453–75. https://doi.org/10.1016/j.enconman.2014.05.003.

[17] Liu Y, Abu-Rub H, Ge B, Blaabjerg F, Ellabban O, Loh PC. Impedance Source Power Electronic Converters. Chichester, U.K: John Wiley & Sons; 2016.

[18] Olatomiwa L, Mekhilef S, Ismail MS, Moghavvemi M. Energy management strategies in hybrid renewable energy systems: a review. Renew Sustain Energy Rev 2016;62:821–35. https://doi.org/10.1016/j.rser.2016.05.040.

[19] Simon D, Member S. Biogeography-based optimization. IEEE Trans Evol Comput 2008;12:702–13. https://doi.org/10.1109/TEVC.2008.919004.

[20] Farajdadian S, Hosseini SMH. Optimization of fuzzy-based MPPT controller via metaheuristic techniques for stand-alone PV systems. Int J Hydrogen Energy 2019;44(47):25457–72. https://doi.org/10.1016/j.ijhydene.2019.08.037.

[21] Kumaran J, Ravi G. Long-term sector-wise electrical energy forecasting using artificial neural network and biogeography-based optimization. Electr Power Components Syst 2015;43(11):1225–35. https://doi.org/10.1080/15325008.2015.1028115.

[22] Liu K, Zou C, Li K, Wik T. Charging pattern optimization for lithium-ion batteries with an electrothermal-aging model. IEEE Trans Ind Informatics 2018;14(12):5463–74. https://doi.org/10.1109/TII.2018.2866493.
[23] SunPower. X-Series Residential Solar Panels. X21-335-BLK. Available from: <https://us.sunpower.com/sites/default/files/sunpower-x-series-residential-solar-panels-x21-335-blk-x21-345-datasheet-504828-revg.pdf> [accessed September 2020].
[24] HOPPECKE Power VR L. Available from: https://www.hoppecke.com/es/producto/grid-power-vr-l/> [accessed December 2020].
[25] International Hydrail Conference. HyPM™ Fuel Cell Power Modules & Systems. Available from: https://hydrail.appstate.edu/sites/hydrail.appstate.edu/files/9_Kammerer.pdf [accessed September 2020].
[26] Proton Energy. C Series Hydrogen Generation Systems. Available from: https://www.protonenergy.com/sites/default/files/2017-07/PD-0600-0068-rev%20F.pdf [accessed September 2020].
[27] Commission IE. IEC 61851-1: 2017 Electric vehicle conductive charging system-Part 1: General requirements. 2017. Geneva, Switzerland.
[28] De Oliveira-Assis L, Soares-Ramos EPP, Sarrias-Mena R, Garcia-Trivino P, Fernandez-Ramirez LM. Large-Scale Grid Connected Quasi-Z-Source Inverter-Based PV Power Plant. In: Proc. - 2020 IEEE Int. Conf. Environ. Electr. Eng. 2020 IEEE Ind. Commer. Power Syst. Eur. EEEIC / I CPS Eur. 2020; 2020. pp. 1–5.
[29] Ortega M, Ortega MV, Jurado F, Carpio J, Vera D. Bidirectional DC–DC converter with high gain based on impedance source. IET Power Electron 2019;12(8):2069–78. https://doi.org/10.1049/iet-pel.2018.5385.
[30] Soares-Ramos EP, De Oliveira-Assís L, Sarrias-Mena R, Garcia-Triviño P, García-Vázquez CA, Fernández-Ramírez LM. Averaged dynamic modelling and control of a quasi-Z-source inverter for wind power applications. IEEE Access 2021;9:114348–58. https://doi.org/10.1109/ACCESS.2021.3104797.
[31] Liu Y, Ge B, Abu-Rub H, Peng FZ. Overview of space vector modulations for three-phase Z-Source/quasi-z- source inverters. IEEE Trans Power Electron 2014;29(4):2098–108. https://doi.org/10.1109/TPEL.2013.2269539.
[32] Xie C, Ogden JM, Quan S, Chen Q. Optimal power management for fuel cell-battery full hybrid powertrain on a test station. Int J Electr Power Energy Syst 2013;53:307–20. https://doi.org/10.1016/j.ijepes.2013.05.016.
[33] Huang CN, Chen YS. Design of magnetic flywheel control for performance improvement of fuel cells used in vehicles. Energy 2017;118:840–52. https://doi.org/10.1016/j.energy.2016.10.112.
[34] Rezzak D, Boudjerda N. Robust energy management strategy based on non-linear cascade control of fuel cells-super capacitors hybrid power system. Int J Hydrogen Energy 2020;45(43):23254–74. https://doi.org/10.1016/j.ijhydene.2020.05.250.
[35] Pukrushpan JT, Stefanopoulou AG, Peng H. Control of fuel cell power systems: principles, modeling, analysis and feedback design. London, U.K: Springer Science & Business Media; 2004.
[36] Sarrias-Mena R, Fernández-Ramírez LM, García-Vázquez CA, Jurado F. Electrolyzer models for hydrogen production from wind energy systems. Int J Hydrogen Energy 2015;40(7):2927–38. https://doi.org/10.1016/j.ijhydene.2014.12.125.
[37] Atlam O, Kolhe M. Equivalent electrical model for a proton exchange membrane (PEM) electrolyser. Energy Convers Manag 2011;52(8-9):2952–7. https://doi.org/10.1016/j.enconman.2011.04.007.
[38] Dufo-López R, Cortés-Arcos T, Artal-Sevil JS, Bernal-Agustín JL. Comparison of lead-acid and li-ion batteries lifetime prediction models in stand-alone photovoltaic systems. Appl Sci 2021;11:1–16. https://doi.org/10.3390/app11031099.
[39] SimPowerSystems TM. Reference. Natick, MA: Hydro-Québec and the MathWorks. Inc; 2015.
[40] De Soto W, Klein SA, Beckman WA. Improvement and validation of a model for photovoltaic array performance. Sol Energy 2006;80(1):78–88. https://doi.org/10.1016/j.solener.2005.06.010.
[41] Villalva MG, Gazoli JR, Filho ER. Comprehensive approach to modeling and simulation of photovoltaic arrays. IEEE Trans Power Electron 2009;24(5):1198–208. https://doi.org/10.1109/TPEL.2009.2013862.
[42] Lang Z, Zhang Y. Parameter identification and performance estimation for PV modules based on reduced forms model. J Renew Sustain Energy 2020;12(5):053703. https://doi.org/10.1063/5.0019511.
[43] Xu L, Li J, Hua J, Li X, Ouyang M. Adaptive supervisory control strategy of a fuel cell/battery-powered city bus. J Power Sources 2009;194(1):360–8. https://doi.org/10.1016/j.jpowsour.2009.04.074.
[44] Torreglosa JP, Jurado F, García P, Fernández LM. Hybrid fuel cell and battery tramway control based on an equivalent consumption minimization strategy. Control Eng Pract 2011;19(10):1182–94. https://doi.org/10.1016/j.conengprac.2011.06.008.
[45] Yazdani A, Iravani R. Voltage-sourced converters in power systems: modeling, control, and applications. Hoboken, New Jersey: EE.UU. John Wiley & Sons; 2010.
[46] García P, Torreglosa JP, Fernández LM, Jurado F. Improving long-term operation of power sources in off-grid hybrid systems based on renewable energy, hydrogen and battery. J Power Sources 2014;265:149–59. https://doi.org/10.1016/j.jpowsour.2014.04.118.